Bull. Chem. Soc. Jpn., 73, 2185—2192 (2000)

Hydrogen Abstraction Reactions from C_2 Hydrocarbons

Nílson Kunioshi,* Shigeru Mouri, Noriyuki Yamashita, and Seishiro Fukutani

Department of System Engineering, Okayama Prefectural University, 111 Kuboki, Soja 719-1197

(Received November 4, 1999)

The sequence of hydrogen abstraction reactions from ethane to acetylene, which proceeds in fuel-rich methane flames, has been investigated by an ab initio molecular orbital method. First, the hydrogen abstraction mechanism was elucidated through an analysis of the variation in the electron spin density distributions through the reacting species. The H atoms holding the largest spin densities within a radical where seen to be those being abstracted from the species. The reaction rate coefficients for the four elementary abstraction steps from ethane to acetylene were determined through the transition state theory, and the results were compared with data published in the literature. The obtained rate coefficients were found to be lower than the published data for all four reactions examined. Especially, for two of the reactions, some published data seem to be too large, considering that the rate coefficients obtained through transition state theory tend to be larger than the true values.

Methane, the main component of natural gas, is known to be oxidized through two different routes: the C_1 route, which comprises reactions that proceed through species containing only one carbon atom, and the C_2 route, which comprises reactions that proceed through species containing two carbon atoms. The C_1 route is predominant under lean conditions, and the C_2 route predominates under stoichiometric and fuel-rich conditions.[1—3] The first step in methane combustion is necessarily the production of CH_3 radicals, from which the combustion reactions can proceed into the two routes cited above. When O atoms are abundant, as under lean conditions, CH_3 is oxidized into HCHO, and reactions belonging to the C_1 route occur, through $CH_4 \rightarrow CH_3 \rightarrow HCHO \rightarrow CHO \rightarrow CO \rightarrow CO_2$. Under methane-rich conditions, the concentration of O atoms in the flame is low, and only a small part of the CH_3 radicals initially formed is oxidized into HCHO; the CH_3 radicals combine with themselves into C_2H_6, and the C_2 route is started. From C_2H_6, a sequence of H abstraction reactions occurs, through $C_2H_6 \rightarrow C_2H_5 \rightarrow C_2H_4 \rightarrow C_2H_3 \rightarrow C_2H_2$. During the final steps of the C_2 route C_2H_2 is formed, which can be oxidized by O atoms into CO;[4] but when the supply of oxygen to the fuel is too small, acetylene is not oxidized, and plays an important role in the formation of polycyclic aromatic hydrocarbons (PAH),[5] the precursor species to soot. The hydrogen abstraction reactions in the C_2 route thus lead to the formation of double and triple bonds from single bonds, and species having carbon atoms linked by double and triple bonds are suitable to participate in combustion synthesis reactions (flame reactions in which the number of carbon atoms grow in the molecule). This is the reason for the presence of molecules as large as PAH in flames of a fuel so simple as methane. The C_2 route is therefore very important not only for governing the mechanism of partial combustion of methane, but also for being a route forming species which promote combustion synthesis reactions in hydrocarbon flames. Good knowledge concerning the elementary steps belonging to the C_2 route is thus a requisite for any detailed comprehension of the combustion mechanism of hydrocarbons. Although kinetic data about these reactions are found in the literature, discrepancies among the experimental results are seen, as pointed out by Warnatz[6] in his compilation of rate constants for reactions in the C/H/O system. In addition, hydrogen abstraction and C_2H_2 addition reactions constitute the HACA (H abstraction-C_2 addition) mechanism, through which PAH molecules grow in size in sooting hydrocarbon flames.[5,7,8] Therefore, good knowledge of hydrogen abstraction reactions is important in predicting PAH growth reactions.

In this work, the main elementary steps in the C_2 route, which are hydrogen abstraction reactions, were treated theoretically through an ab initio molecular orbital method; also, their rate coefficients were calculated and compared with values published in the literature.

Theoretical

The calculations were performed using Gaussian98.[9] The variations in the energy and molecular structure with the intrinsic reaction coordinate were obtained at the MP2/6-31G(d,p) level. For a more precise evaluation of the activation energies, the G2M method[10] was used. Under this method, the calculation level is highered to B3LYP/6-311G(d,p), with reoptimization of the structures of the transition states and reactants. Because the B3LYP level of calculation treats the electron correlation in a more precise manner than does the MP2 level, the optimized geometries and the vibrational frequencies required to evaluate the zero-point energies and partition functions are expected to be more accurate. In addition to using the B3LYP/6-311G(d,p) optimized geometries, the G2M method evaluates and minimizes errors by comparing the energies yielded from different levels of calculation:

$$E(\mathrm{G2M}) = E_{\mathrm{bas}} + \Delta E(+) + \Delta E(\mathrm{2df}) + \Delta E(\mathrm{CC}) + \Delta + \Delta \mathrm{E(HLC)} + \mathrm{ZPE}, \quad (1)$$

where

$$E_{\mathrm{bas}} = E[\mathrm{PMP4/6\text{-}311G(d,p)}], \quad (2)$$

$$\Delta E(+) = E[\mathrm{PMP4/6\text{-}311+G(d,p)}] - E_{\mathrm{bas}}, \quad (3)$$

$$\Delta E(\mathrm{2df}) = E[\mathrm{PMP4/6\text{-}311G(2df,p)}] - E_{\mathrm{bas}}, \quad (4)$$

$$\Delta E(\mathrm{CC}) = E[\mathrm{CCSD(T)/6\text{-}311G(d,p)}] - E_{\mathrm{bas}}, \quad (5)$$

$$\Delta = E[\mathrm{UMP2/6\text{-}311+G(3df,2p)}] - E[\mathrm{UMP2/6\text{-}311G(2df,p)}] - E[\mathrm{UMP2/6\text{-}311+G(d,p)}] + E[\mathrm{UMP2/6\text{-}311G(d,p)}], \quad (6)$$

$$\Delta E(\mathrm{HLC}) = -5.78 n_\beta - 0.19 n_\alpha \quad (7)$$

In the above equations, n_α and n_β are the number of α-spin and β-spin electrons, respectively, and ZPE is the zero-point energy calculated at the B3LYP/6-311G(d,p) level. The uncertainty in E(G2M) is stated to be within ± 8 kJ mol^{-1}.[10]

The rate coefficients are calculated through transition state theory,[11]

$$k = L^\ddagger \frac{k_B T}{h} \frac{Q^\ddagger Q_{\mathrm{tunnel}}}{Q_A Q_B} \exp(-E_0/k_B T), \quad (8)$$

where $L^\ddagger$ is the number of transition states of equivalent structure; $Q^\ddagger$, Q_A, and Q_B are the partition functions for the transition state and the reactants A and B, respectively; and E_0 is the activation energy. The partition functions were evaluated under B3LYP/6-311G(d,p), and the activation energy through the G2M method. The tunneling effect, expected to be important in reactions in which hydrogen atoms play a central role, is evaluated through[12]

$$Q_{\mathrm{tunnel}} = 1 - \frac{1}{24}\left(\frac{h\nu_s}{k_B T}\right)^2 \left(1 + \frac{k_B T}{E_0}\right), \quad (9)$$

where ν_s is the imaginary vibration frequency of the transition state, evaluated here at the B3LYP/6-311G(d,p) level.

The calculated rate coefficients were compared with the kinetic data of Warnatz,[6] who recommends rate coefficients based on the consideration of a large number of experimental data and also, when available, with the rate coefficients in the GRI-mech 3.0 scheme.[13] The Warnatz rate coefficients have been adopted in previous studies,[2,3] and were found to give good results, although no comparison between the flame velocities predicted by that scheme and experimental values was made.

Results and Discussion

The results obtained from an IRC calculation under MP2/6-31G(d,p) for the sequence of hydrogen abstraction reactions from C_2H_6 to C_2H_2 are shown in Fig. 1. The energy plotted in Fig. 1 is that of the system relative to the C_2H_6 + H state before reaction. The energy is seen to change smoothly and to increase as the H abstraction proceeds through

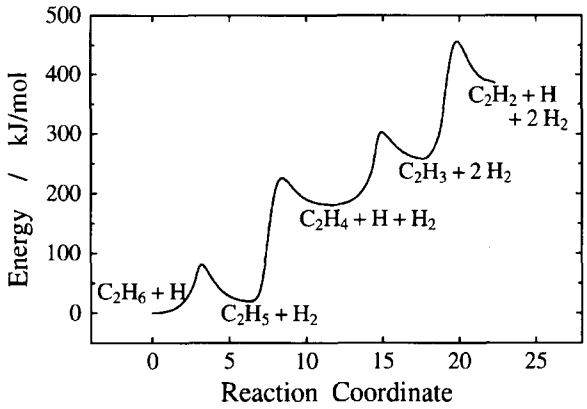

Fig. 1. Change in energy as H abstraction reactions proceed through $C_2H_6 \rightarrow C_2H_5 \rightarrow C_2H_4 \rightarrow C_2H_3 \rightarrow C_2H_2$.

$C_2H_6 + H \rightarrow C_2H_5 + H_2$	R1
$C_2H_5 \rightarrow C_2H_4 + H$	R2
$C_2H_4 + H \rightarrow C_2H_3 + H_2$	R3
$C_2H_3 \rightarrow C_2H_2 + H$	R4

The final state, that corresponding to the products of reaction R4, is C_2H_2+H. However, considering that the H_2 molecules formed through R1 and R3 remain in the system, in fact the final state is C_2H_2+2 H_2+H. An estimation of the difference in energy between this final state and the initial C_2H_6+H state requires knowing the energy of an isolated H_2 molecule. Because the same G2M method applied to the reactants, transition states, and products of reactions R1 to R4 cannot be applied in determining the energy of an H_2 molecule, the G2M energy for H_2 was evaluated as the difference between the G2M energies for C_2H_5+H_2 and C_2H_5. The so-calculated difference in G2M energies between the final and initial states is 308.8 kJ mol^{-1}. In order to compare with experimental enthalpies, the thermal enthalpies at 298.15 K were included in the ZPE of Eq. 1. Actually, in the C_2H_5+H_2 state these two species interact, so that the magnitude of the energy for the isolated H_2 is overestimated, and the difference in energy between the final and initial states is underestimated. Because an evaluation of the interaction energy between C_2H_5 and H_2 under MP2/6-31G(d,p) gave a value of about 1.9 kJ mol^{-1}, the estimated energy difference mentioned above increases to 312.6 kJ mol^{-1} if the MP2 energy is just multiplied by 2 and added to the G2M value. Tabulated enthalpies of formation[14] at 298.15 K give an energy difference of 311.4 kJ mol^{-1} between the final and initial states of Fig. 1, so that the difference between the G2M energy gap and the tabulated value is just 1.2 kJ mol^{-1}. This confirms that the G2M method is able to give accurate energies.

In the energy changes for the four abstraction reactions shown in Fig. 1, the resemblance between reactions R1 and R3, and that between reactions R2 and R4 are obvious. In reactions R1 and R3, the H abstraction occurs through an attack of an H atom, while R2 and R4 are unimolecular dissociation reactions. Although the OH radicals and O atoms could be thought of as alternative reactants to attack C_2H_6 and C_2H_4,

previous studies on methane-air flames under rich conditions showed that H abstraction reactions from C_2H_6 and C_2H_4 occur preferentially with an attack of H atoms.[2] Furthermore, although H abstraction from C_2H_5 and C_2H_3 could also be promoted with an attack of H atoms and other species, the same previous results showed that H dissociation from those radicals proceed faster than other abstraction channels. Because reactions R2 and R4 are pressure-dependent, under atmospheric and moderate pressures, those dissociation reactions are promoted by a third body: $C_2H_5+M \rightarrow C_2H_4+H+M$ and $C_2H_3+M \rightarrow C_2H_2+H+M$, respectively. The rate coefficients of such third-body reactions are expressed as functions of pressure, the rate coefficients of the high-pressure limit reactions, R2 and R4, studied here, and the low-pressure limit rate coefficients, according, for example, to the Troe-form fall-off functions.[15]

Not considering, for now, the zero-point energies, Fig. 1 shows that the activation energy of reaction R1 is about 81.0 kJ mol^{-1} and that of reaction R3 is 122.2 kJ mol^{-1}. The activation energy for the H abstraction from C_2H_4 is larger than that for abstraction from C_2H_6, as can be expected from the fact that the C–H bond strength in C_2H_4 is larger than that in C_2H_6. In addition, the activation energies for the dissociation reactions of C_2H_5 (R2) and C_2H_3 (R4) are, respectively, 204.4 and 198.9 kJ mol^{-1}, close to each other and much greater than those of reactions R1 and R3.

In the following, each abstraction step will be discussed in detail.

R1: $C_2H_6 + H \rightarrow C_2H_5 + H_2$. The arrangement of the atoms in the reactants, transition state and products is shown along with the correspondent electron spin densities in Fig. 2. Since the two electrons in a covalent bond have each a positive and a negative spin, if the bond is stable the spins cancel and the spin density there is zero. The sites in a molecular system showing high spin density are those holding an unpaired electron or an electron pair partially split; Fig. 2(a) shows that the attacking H atom holds an unpaired electron and that all electrons in the ethane molecule are paired in stable bonds. As the attacking H atom becomes closer to the ethane molecule, a splitting of the electron pair in a C–H bond is induced, so that the spin density there is no longer zero. The situation at the transition state is depicted in Fig. 2(b). Hereafter, the molecule is symmetric to the plane of the figure, with two H atoms lying just above two other H atoms, which cannot be seen in the figure. The H atom of the ethane molecule, being pulled by the approaching H atom, is seen to become apart from the C atom. Already at this stage, that C atom tends to become an sp^2 carbon, lying almost in the same plane as that defined by the three atoms (two H and one C) linked to it. The carbon orbital participating in the stretched C–H bond then tends to become a $2p_z$ orbital, orthogonal to the sp^2 plane. The spin densities at the transition state show that the negative-spin electron of the H atom is surrounded by two positive-spin electrons, so that it can be paired with either of them. If the atomic vibrations favor the reaction to proceed further in the forward direction, the pairing is with the electron of the attacking H atom and the $C_2H_5+H_2$ form, as shown in Fig. 2(c). In that structure, the unpaired electron is located in the C atom, which initially held the H atom that was abstracted, and a slightly positive spin density remains in one of the H atoms of the H_2 molecule. As H_2 separates from C_2H_5, its spin density vanishes.

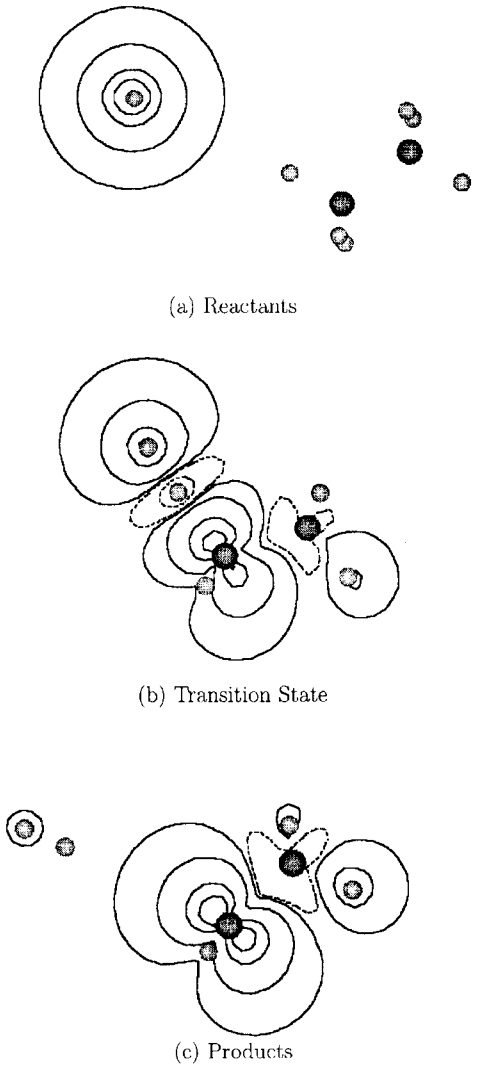

(a) Reactants

(b) Transition State

(c) Products

Fig. 2. Change in atomic arrangement and spin density distribution during reaction $C_2H_6+H \rightarrow C_2H_5+H_2$. Solid contours indicate positive spin densities of 0.001, 0.01, 0.05, and 0.1 Å^{-3}, and dashed contours negative spin densities of -0.001 and -0.01 Å^{-3}. Hereafter, C atoms are represented by larger and darker spheres, and H atoms by smaller and lighter spheres.

An accurate determination of the activation energy of reaction R1 requires a good evaluation of the energies of the reactants and the transition state with consideration of the zero-point energies. The G2M activation energy for R1 was found to be $E_0 = 47.7$ kJ mol^{-1}; the imaginary frequency of vibration at the transition state was $\nu_s = 1181i$ cm^{-1}. Using these values and evaluating Eqs. 8 and 9 at 298.15 K, 333 K, 363 K, 400 K, 444 K, 500 K, 571 K, 666 K, 800 K, 1000 K, 1333 K, and 2000 K, the values for the rate coefficient

of reaction R1 were obtained (Fig. 3). For a comparison, the rate coefficient recommended by Warnatz[6] and that in the GRI-mech 3.0 scheme[13] are also included in the figure. Because R1 was seen to occur at temperatures not lower than 1000 K at the inner cone of a bunsen methane-air flame,[2] the temperature range of interest is just that in which the calculated rate constant is closest to the literature rate coefficients. It should be noted that Q_{tunnel} is about 2 at temperatures of around 300 K, but at temperatures around 1000 K and higher it is smaller than 1.1 for all of the four reactions investigated; thus, in the temperature range of interest the effect of tunneling is small. A least-squares fitting into the results calculated here above 800 K led to $k_1 = 2.14\times10^{10}\ T^{1.15}\ \exp(-43.4\ \text{kJ mol}^{-1}/RT)$ (hereafter, all the reaction coefficients are in units of mol, cm, s), while the expressions of Warnatz and GRI are, respectively, $5.4\times10^{2}\ T^{3.5}\exp(-21.8\ \text{kJ mol}^{-1}/RT)$ and $1.15\times10^{8}\ T^{1.9}\ \exp(-31.5\ \text{kJ mol}^{-1}/RT)$. Figure 3 shows that the rate coefficients calculated here are slightly smaller than the literature values; at 2000 K the calculated coefficient is 1/3.5 of the GRI's and 1/5 of the Warnatz' value.

R2: $C_2H_5 \rightarrow C_2H_4 + H$. Figure 4 shows the changes in the atomic arrangement and spin-density distribution during reaction R2. Here, from the beginning of the reaction the molecular system is symmetric with respect to the plane of the figure, which intercepts the two C atoms and the lowest H atom in Fig. 4(a). The other two visible H atoms are above the plane, and lie just above other two H atoms, which are not visible in the figure. The unpaired electron is in a $2p_z$ orbital of the left-side C atom. But it can be seen that the H atom which lies in the plane of the figure also shows a positive electron spin density, with the C atom linked to it having a negative spin density. This is due to the hyperconjugation effect arising from the fact that the C–H bond in question and the $2p_z$ orbital holding the unpaired electron are approximately parallel to each other. As a result, the unpaired electron in the $2p_z$ orbital induces a splitting of the electron pair in that C–H bond, and the transition state shown in Fig. 4(b) is formed. There, the highest positive spin density is already at the H atom. The negative spin density at the right-side C atom is of the same magnitude as that of the positive spin density at the left-side C atom and, depending on the vibrations of the molecular system, the H atom can be released and the C atoms can share with each other their positive-spin and negative-spin electrons to form a π bond. In this way, the C_2H_4+H depicted in Fig. 4(c) form.

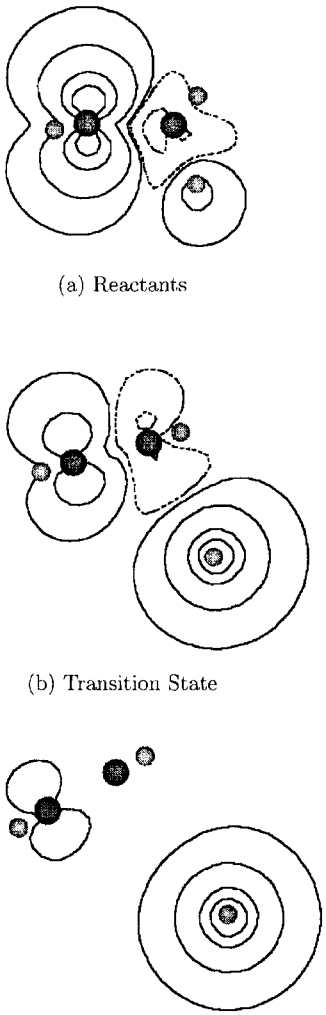

Fig. 4. Change in atomic arrangement and spin density distribution during reaction $C_2H_5 \rightarrow C_2H_4+H$. Solid contours indicate positive spin densities of 0.001, 0.01, 0.05, and 0.1 Å^{-3}, and dashed contours negative spin densities of -0.001 and $-0.01\ \text{Å}^{-3}$.

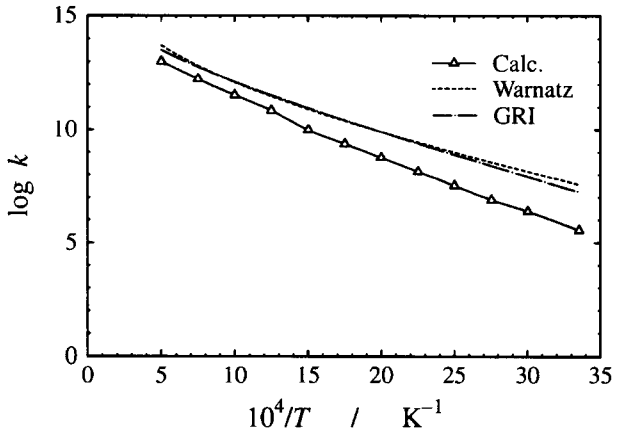

Fig. 3. Arrhenius plot for the rate coefficient of the reaction $C_2H_6+H \rightarrow C_2H_5+H_2$ calculated here (Calc.), in comparison with data of Warnatz[6] and the GRI-Mech 3.0 scheme.[13] k is in units of $\text{cm}^3\ \text{mol}^{-1}\ \text{s}^{-1}$.

The H atom holding the largest spin density in C_2H_5 is then the one which is abstracted from the radical.

The G2M activation energy for R2 was evaluated as 152.1 kJ mol^{-1}. And with the imaginary frequency at the transition state, $309i\ \text{cm}^{-1}$, the rate coefficients evaluated at the same temperatures mentioned above led to the results plotted in Fig. 5. The calculated coefficient is again lower than that of Warnatz by a factor of 70 at 2000 K. As determined by the transition state theory, because the obtained results are expected to be larger than the true rate coefficients,[11] the Warnatz coefficient seems to be too large. A fitting into the calculated results gave $k_2 = 5.00\times10^{14}$

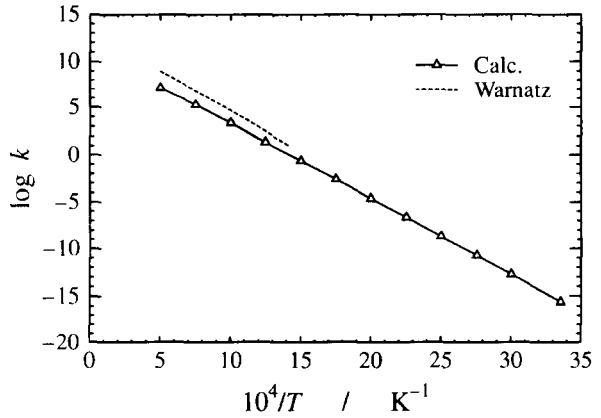

Fig. 5. Arrhenius plot for the rate coefficient of the reaction $C_2H_5 \rightarrow C_2H_4+H$. k is in units of s^{-1}.

$T^{-1.04}\exp(-158.3\ \text{kJ mol}^{-1}/RT)$, while the Warnatz recommendation is $2.0\times10^{13}\exp(-166.0\ \text{kJ mol}^{-1}/RT)$.

R3: $C_2H_4 + H \rightarrow C_2H_3 + H_2$. As shown in Fig. 6, in this reaction all of the atoms remain in the same plane from the beginning of the interaction between the reactants throughout the formation of the products. As the H atom approaches the ethylene molecule (Fig. 6(a)), it induces a partial split of the electron pair of a C–H bond, and the transition state shown in Fig. 6(b) is formed. If the atomic vibrations support the reaction to proceed further in the forward direction, an H_2 molecule and a vinyl radical are formed, as displayed in Fig. 6(c). The unpaired electron occupies an sp^2 orbital in C_2H_3, and an induced positive spin density is seen in both H atoms of the CH_2 side of the radical. Reaction R3 proceeds through a mechanism similar to that of reaction R1, with the attacking H atom inducing a splitting in the electron pair of a C–H bond. In both reactions R1 and R3, because no spin density exists in the hydrocarbon in the state previous to reaction, an approaching reactive species is necessary for the hydrogen abstraction to proceed at significant rates.

From the obtained G2M activation energy of 68.2 kJ mol^{-1} and the imaginary frequency of $936i$ cm^{-1} at the transition state, the rate coefficients were calculated at various temperatures and plotted in Fig. 7. Again, the present results are lower than the literature values, but here the agreement is closer: at 2000 K, the data of Just et al.,[16] GRI, Warnatz, and Bhargava[17] are about 2-times larger; at 1333 K the coefficient of Skinner et al.[18] is 1.6-times larger than the present results. A least-squares fitting based on the results for the temperature range above 800 K (the range of interest and for which experimental data are available) led to $k_3 = 2.63\times10^8 T^{1.87}\exp(-65.8\ \text{kJ mol}^{-1}/RT)$, while the Warnatz coefficient is $1.5\times10^{14}\exp(-42.70\ \text{kJ mol}^{-1}/RT)$. The GRI rate coefficient, expressed as $1.32\times10^6 T^{2.5}\exp(-51.2\ \text{kJ mol}^{-1}/RT)$, agrees with the data of Just et al.,[16] Bhargava and Westmoreland,[17] and Skinner et al.,[18] being much lower than the recommendation of Warnatz. The rate coefficients calculated here for reaction R3 thus support the GRI and Bhargava rate coefficients. Warnatz seems to have relied on the data of Benson[19] and Peters,[20] because his recommended rate coefficient lies between those experimental data (not displayed in the figure to make it more clear).

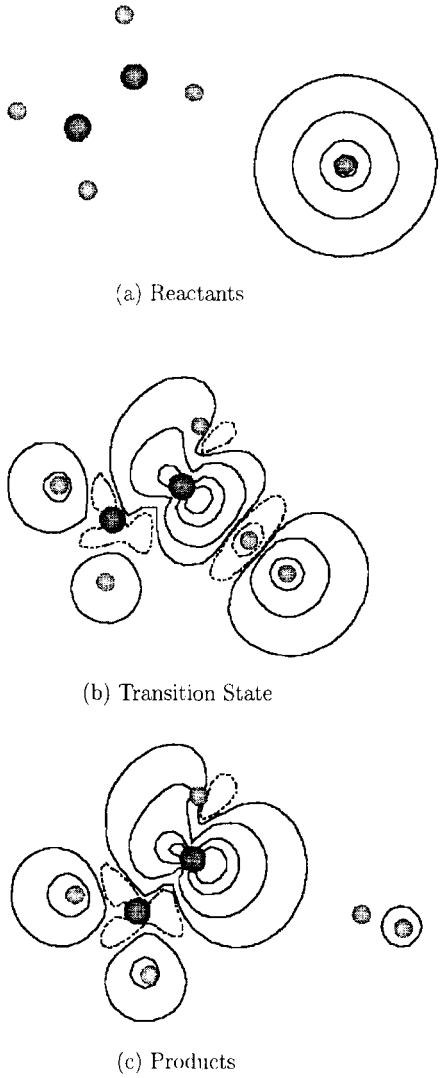

(a) Reactants

(b) Transition State

(c) Products

Fig. 6. Change in atomic arrangement and spin density distribution during reaction $C_2H_4+H \rightarrow C_2H_3+H_2$. Solid contours indicate positive spin densities of 0.001, 0.01, 0.05, and 0.1 Å^{-3}, and dashed contours negative spin densities of -0.001 and -0.01 Å^{-3}.

R4: $C_2H_3 \rightarrow C_2H_2 + H$. In this reaction, all atoms continue to lie in the same plane. As already mentioned, in the vinyl radical both H atoms at the CH_2 side hold a positive spin density, with the H atom at the left hand side of Fig. 8(a) having a higher density than the H atom at the right. The electron pair in the C–H bond involving the former H atom is therefore the most split within C_2H_3. At the transition state, Fig. 8(b), an electron of positive spin and an electron of negative spin are in orbitals that belong to neighboring C atoms and are parallel to each other; if the reaction proceeds further in the forward direction, those electrons combine into a π bond to form C_2H_2, and an H atom is released with the unpaired electron (Fig. 8(c)). The H abstraction mechanism is therefore similar to that of reaction R2, in the sense that the electron pair in the C–H bond to be broken is already partially split before reaction, with no need of help from any

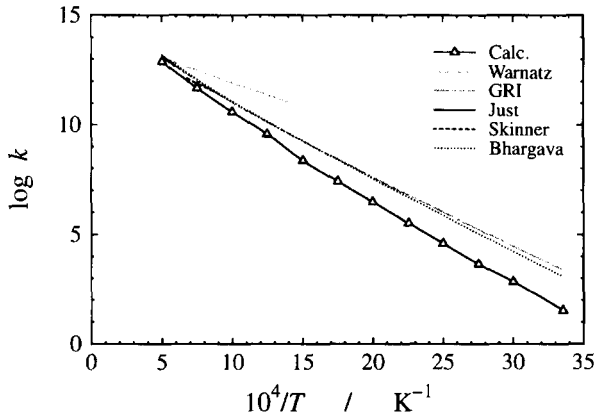

Fig. 7. Arrhenius plot for the rate coefficient of the reaction $C_2H_4+H \rightarrow C_2H_3+H_2$. In addition to the rate data recommended by Warnatz[6] and GRI-mech 3.0 scheme,[13] data from Just et al.,[16] Bhargava and Westmoreland,[17] Skinner et al.,[18] are also plotted for comparison. k is in units of $cm^3\,mol^{-1}\,s^{-1}$.

attacking species.

The H atom to be abstracted from C_2H_3, as in the case of C_2H_5, is the one that has the largest spin density. The case of larger radicals is discussed in the next section.

The rate coefficients for R4, calculated from the obtained G2M activation energy of 161.0 kJ mol^{-1} and imaginary frequency of 592*i* cm^{-1} at the transition state, are plotted in Fig. 9. A least-squares fitting on the calculated results leads to the expression $k_4 = 5.80\times10^{14}\ T^{-0.66}\exp(-162.5\ \text{kJ mol}^{-1}/RT)$, while the Warnatz expression is $1.6\times10^{14}\exp(-159.0\ \text{kJ mol}^{-1}/RT)$. At 2000 K, the Warnatz rate coefficient is 52-times larger than the value calculated here. This discrepancy seems to be sufficiently large to state that the Warnatz coefficient is too large, as in the two previous reactions.

HACA Reactions.

Hydrogen abstraction, along with C_2H_2 addition, constitutes the HACA (H abstraction-C_2 addition) mechanism, by which PAH molecules are stated to grow in size in sooting hydrocarbon flames.[7,8] According to the HACA mechanism, phenyl radical (C_6H_5) growth into 1-naphthyl radical ($C_{10}H_7$) proceeds as illustrated in Fig. 10. The two emphasized H atoms in styryl radical (the product of step 1) are abstracted with the formation of phenylacetylene (the product of step 2) through step 2 proceeding first. The electron spin-density distribution through styryl radical plotted in Fig. 11 shows that the H atom holding the largest density is the one that does undergo abstraction. Experimental evidence, including an observation of phenylacetylene in flames,[21] supports the HACA predictions. Thus, also in this typical HACA reaction, the H atom undergoing abstraction from a radical is the one that holds the largest spin density among all H atoms. Cases of reactions of PAH formation in which no π bonds form after an H abstraction are being investigated;[22] further insights on the relation between the spin density around an H atom and the propensity of that atom to be abstracted from

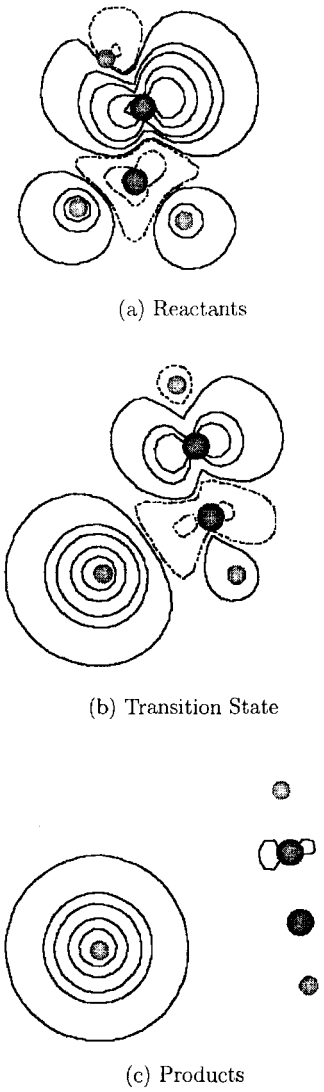

(a) Reactants

(b) Transition State

(c) Products

Fig. 8. Change in atomic arrangement and spin density distribution during reaction $C_2H_3 \rightarrow C_2H_2+H$. Solid contours indicate positive spin densities of 0.001, 0.01, 0.02, 0.05, and 0.1 Å^{-3}, and dashed contours negative spin densities of -0.001 and -0.01 Å^{-3}.

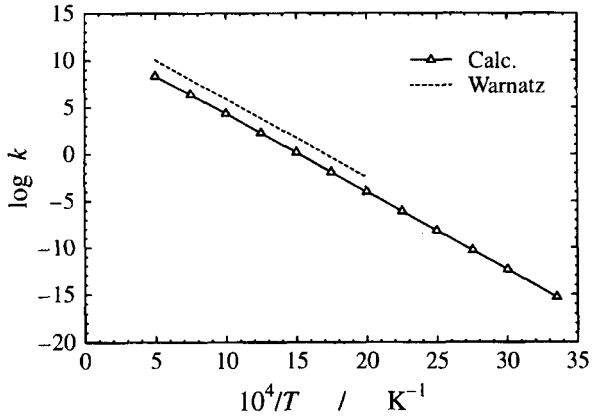

Fig. 9. Arrhenius plot for the rate coefficient of the reaction $C_2H_3 \rightarrow C_2H_2+H$. k is in units of s^{-1}.

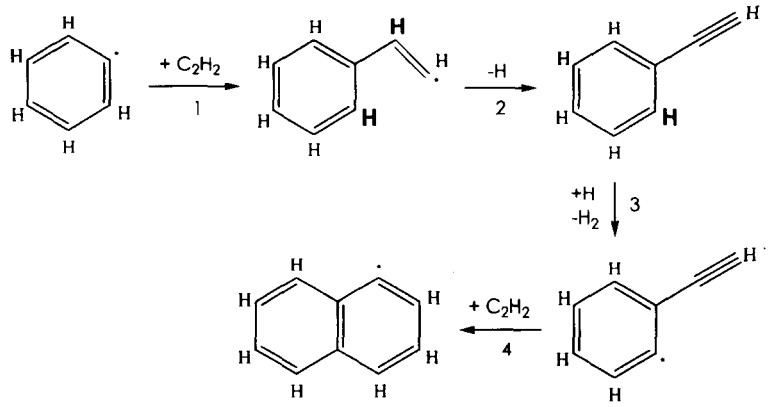

Fig. 10. Growth from phenyl radical to 1-naphthyl radical through H abstraction–C_2H_2 addition (HACA) mechanism.

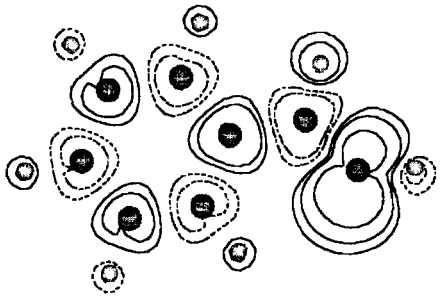

Fig. 11. Electron spin density distribution in styryl radical. Solid contours indicate positive spin densities of 0.005, 0.01, and 0.03 $Å^{-3}$, and dashed contours negative spin densities of −0.005 and −0.01 $Å^{-3}$.

a radical can be expected.

Summary. The sequence of H abstraction reactions, which are the main steps in the C_2 route which proceeds in fuel-rich methane flames, were analyzed in detail by an ab initio molecular orbital method. The obtained results can be summarized as follows:

1. The four H abstraction steps from ethane to acetylene can be divided into two pairs of similar reaction mechanism: the H abstraction from stable ethane and ethylene proceeds through the attack of an H atom, and that from the radicals C_2H_5 and C_2H_3 are unimolecular dissociation reactions. Paired reactions have similar activation energies and rate coefficients.

2. H abstraction from ethane and ethylene requires an attacking reactive species to promote C–H bond breaking. The attacking H atom induces a splitting of the electron pair in the C–H covalent bond to be broken, and the reaction proceeds with the release of a stable H_2 molecule. H abstraction from radicals does not require any attacking species, because the electron pair in the C–H bond to be broken is already partially split into positive and negative spin-density sites. The splitting is induced in a C–H bond whose orientation is nearly parallel to the orbital holding the unpaired electron; the abstraction reaction proceeds with the formation of a stable π bond and the release of an H atom that carries away the unpaired electron.

3. The H atom being abstracted from C_2H_5 and C_2H_3 was the one holding the largest spin density among all H atoms in the species. This was also the case in styryl radical, a typical intermediary in the growth mechanism of PAH (polycyclic aromatic hydrocarbon) molecules, which proceeds in rich hydrocarbon flames.

4. The rate coefficients for the four abstraction steps R1 to R4 were calculated through transition state theory, and can be expressed by:

$$k_1 = 2.14 \times 10^{10} T^{1.15} \exp(-43.4\ \text{kJ mol}^{-1}/RT),$$
$$k_2 = 5.00 \times 10^{14} T^{-1.04} \exp(-158.3\ \text{kJ mol}^{-1}/RT),$$
$$k_3 = 2.63 \times 10^{8} T^{1.87} \exp(-65.8\ \text{kJ mol}^{-1}/RT),$$
$$k_4 = 5.80 \times 10^{14} T^{-0.66} \exp(-162.5\ \text{kJ mol}^{-1}/RT).$$

The calculated rate coefficients mentioned here are smaller than the values given in the literature for all four reactions, but for R1 and R3 the agreement is closer than for R2 and R4. Since the rates obtained through the transition state theory are expected to be larger than the true values,[11] the rate coefficients recommended by Warnatz[6] for reactions R2, R3 and R4 are concluded to be too high. For R3, good agreement was obtained with the rate coefficients from GRI[13] and Bhargava.[17] A flame simulation employing the rate coefficients calculated here is in progress[23] in order to observe the flame velocities in methane–air flames resulting from the present results under a broad range of equivalence ratios, and also for peaking up other important elementary reactions for a detailed analysis.

References

1 S. Fukutani, K. Sakaguchi, N. Kunioshi, and H. Jinno, *Bull. Chem. Soc. Jpn.*, **64**, 1623 (1991).

2 N. Kunioshi and S. Fukutani, *Trans. Jpn. Soc. Mec. Eng. B*, **61**, 4492 (1995) (in Japanese).

3 N. Kunioshi and S. Fukutani, *Trans. Jpn. Soc. Mec. Eng. B*, **62**, 374 (1996) (in Japanese).

4 N. Kunioshi, Y. Yatabe, S. Mouri, and S. Fukutani, *JSME Int. J. B*, **43**, 258 (2000).

5 M. Frenklach, D. W. Clary, W. C. Gardiner, Jr., and S. E. Stein, "Twentieth Symposium (International) on Combustion," The Combustion Institute, Pittsburgh (1984), pp. 887—901.

6 J. Warnatz, in "Combustion Chemistry," ed by W. C. Gardiner, Jr., Springer-Verlag, New York (1984), pp. 197—360.

7 H. Wang and M. Frenklach, *J. Phys. Chem.*, **98**, 11465 (1994).

8 M. Frenklach and H. Wang, in "Soot Formation in Combustion," ed by H. Bockhorn, Springer-Verlag, Berlin (1994), pp. 165—192.

9 M. J. Frisch, G. W. Trucks, H. B. Schlegel, G. E. Scuseria, M. A. Robb, J. R. Cheeseman, V. G. Zakrzewski, J. A. Montgomery, Jr., R. E. Stratmann, J. C. Burant, S. Dapprich, J. M. Millam, A. D. Daniels, K. N. Kudin, M. C. Strain, O. Farkas, J. Tomasi, V. Barone, M. Cossi, R. Cammi, B. Mennucci, C. Pomelli, C. Adamo, S. Clifford, J. Ochterski, G. A. Petersson, P. Y. Ayala, Q. Cui, K. Morokuma, D. K. Malick, A. D. Rabuck, K. Raghavachari, J. B. Foresman, J. Cioslowski, J. V. Ortiz, A. G. Baboul, B. B. Stefanov, G. Liu, A. Liashenko, P. Piskorz, I. Komaromi, R. Gomperts, R. L. Martin, D. J. Fox, T. Keith, M. A. Al-Laham, C. Y. Peng, A. Nanayakkara, C. Gonzalez, M. Challacombe, P. M. W. Gill, B. Johnson, W. Chen, M. W. Wong, J. L. Andres, C. Gonzalez, M. Head-Gordon, E. S. Replogle, and J. A. Pople, "Gaussian 98, Revision A.7," Gaussian, Inc., Pittsburgh, PA (1998).

10 A. M. Mebel, K. Morokuma, and M. C. Lin, *J. Chem. Phys.*, **103**, 7414 (1995).

11 J. I. Steinfeld, J. S. Francisco, and W. L. Hase, "Chemical Kinetics and Dynamics," Prentice Hall, New Jersey (1989), Chap. 10.

12 I. Shavitt, *J. Chem. Phys.*, **31**, 1359 (1959).

13 C. T. Bowman, R. K. Hanson, D. F. Davidson, W. C. Gardiner, Jr., V. Lissianski, G. P. Smith, D. M. Golden, M. Frenklach, and M. Goldenberg, http://www.me.berkeley.edu/gri_mech/.

14 D. R. Lide, "CRC Handbook of Chemistry and Physics," 79th ed, CRC Press (1998), pp. 5-29—5-31.

15 W. C. Gardiner, Jr., and J. Troe, in "Combustion Chemistry," ed by W. C. Gardiner, Jr., Springer-Verlag, New York (1984), pp. 173—196.

16 Th. Just, P. Roth, and R. Damm, "Sixteenth Symposium (International) on Combustion," The Combustion Institute, Pittsburgh (1977), p. 961.

17 A. Bhargava and P. R. Westmoreland, *Combust. Flame*, **113**, 333 (1998).

18 G. B. Skinner, R. C. Sweet, and S. K. Davis, *J. Phys. Chem.*, **75**, 1 (1971).

19 S. W. Benson and G. R. Haugen, *J. Phys. Chem.*, **71**, 4404 (1967).

20 J. Peeters and G. Mahnen, "Combustion Institute European Symposium," p. 969, 1973.

21 S. J. Harris, A. M. Weiner, and R. J. Blint, *Combust. Flame*, **72**, 91 (1988).

22 N. Kunioshi, Y. Kouchiyama, and S. Fukutani, in preparation.

23 N. Kunioshi and S. Fukutani, in preparation.